Publications of the Korean Astronomical Society
32: 257 ∼ 261, 2017 March

pISSN 1225-1534
eISSN 2287-6936
https://doi.org/10.5303/PKAS.2017.32.1.257

NEP-AKARI: EVOLUTION WITH REDSHIFT OF DUST ATTENUATION IN 8 μm SELECTED GALAXIES

V. Buat[1], N. Oi[2], D. Burgarella[1], K. Malek[3,4], H. Matsuhara[2], K. Murata[2], S. Serjeant[5], T. T. Takeuchi[6], M. Malkan[7], C. Pearson[6], and T. Wada[2]

[1]Aix-Marseille Université, CNRS, LAM (Laboratoire d'Astrophysique de Marseille) UMR7326, 13388, Marseille, France
[2]Institute of Space and Astronautical Science, Japan Aerospace Exploration Agency, Sagamihara, Kanagawa 229-8510, Japan
[3]Division of Particle and Astrophysical Science, Nagoya University, Furo-cho, Chikusa-ku, Nagoya 464-8602, Japan
[4]National Centre for Nuclear Research, ul. Hoza 69, 00-681 Warszawa, Poland
[5] The Open University, Milton Keynes, MK7 6AA, UK
[6]Graduate School of Science, Nagoya University, Nagoya, Aichi 464-8602, Japan
[7] University of California, Los Angeles, CA 90095-1547, USA
[8] Rutherford Appleton Laboratory Oxon, OX11 0QX, UK

E-mail: veronique.buat@lam.fr

(Received August 31, 2015; Revised October 20, 2016; Accepted October 20, 2016)

ABSTRACT

We built a 8 μm selected sample of galaxies in the NEP-AKARI field by defining 4 redshift bins with the four AKARI bands at 11, 15, 18 and 24 microns ($0.15 < z < 0.49$, $0.75 < z < 1.34$, $1.34 < z < 1.7$ and $1.7 < z < 2.05$) . Our sample contains 4079 sources, 599 are securely detected with *Herschel*/PACS. Also adding ultraviolet (UV) data from *GALEX*, we fit the spectral energy distributions using the physically motivated code CIGALE to extract the star formation rate, stellar mass, dust attenuation and the AGN contribution to the total infrared luminosity ($L_{\rm IR}$). We discuss the impact of the adopted attenuation curve and that of the wavelength coverage to estimate these physical parameters. We focus on galaxies with a luminosity close the characteristic $L^*_{\rm IR}$ in the different redshift bins to study the evolution with redshift of the dust attenuation in these galaxies.

Key words: Galaxies: IR— Galaxies: evolution

1. INTRODUCTION

The strong impact of dust attenuation and the need to estimate it as accurately as possible has led to numerous investigations on samples of star forming galaxies. Quite naturally these studies focused on galaxies selected either in their UV rest-frame or from their emission in recombination lines and whose detection is strongly affected by the attenuation by dust. The aim of the present work is to perform a complementary study by starting with an infrared (IR) selection since dust reemits the absorbed energy of young stars in this wavelength range. Most of the star formation in the universe can be securely measured in IR up to redshift ~ 2 since dust emission dominates the stellar emission. The question we want to answer is: what is the amount of dust attenuation in these galaxies and how does it compare to the global evolution of dust attenuation in the universe and to the trends found in optically selected samples?

2. SAMPLE SELECTION

The infrared space telescope *AKARI* carried out a deep survey of the North Ecliptic Pole (hereafter NEP-deep) with all the filters of the InfraRedCamera (IRC). We take advantage of the continuous filter coverage in the mid-IR to build a 8μm rest-frame selection following the strategy of Goto et al. (2010). Using the S11, L15, L18W and L24 filters we select galaxies from $z = 0.15$ to $z = 2.05$. The NEP-*AKARI* field was also observed by

Table 1
Values of input parameters used for the SED fitting with CIGALE, see text for details

Parameter	Range
$E(B-V)$	0.02-1
Attenuation law	B12,C00, SMC
IR templates, α	1-3
AGN fraction,frac$_{\rm AGN}$	0-0.5
Stellar populations	
age (old stellar population) t_f	2-11 Gyr
e-folding rate τ	1-5 Gyr
age (young stellar population) $t_{\rm ySP}$	50-500 Myr
stellar mass fraction $f_{\rm ySP}$	0.01-0.2

Herschel with the PACS and SPIRE instrument (P.I. S. Sergeant) and by *GALEX* (P.I. M. Malkan). Given the small number of sources detected with SPIRE we only consider PACS data. UV data are also added to galaxies with redshift lower than 0.925 in order that the NUV filter at 230 nm corresponds to rest-frame wavelength larger than 120 nm. Fluxes at 100 and 160 microns from the PACS images and at 230 nm in the GALEX images were measured with DAOPHOT (Mazyed et al., in preparation). Combining the near to mid IR catalogue of Murata et al. (2013) with the optical data of Oi et al. (2014) and with *GALEX* and *Herschel*/PACS detections, we are able to build the UV to IR spectral energy distributions (SED) of our selected sources. The photometric redshifts are from Oi et al. (2014). The SEDs are analysed with the SED fitting code CIGALE in order to measure physical parameters such as dust attenuation, SFR or stellar masses. The amount of dust attenuation and its evolution in redshift is then measured for our selected sources and compared to the results found in UV selections.

3. FITTING THE SPECTRAL ENERGY DISTRIBUTIONS

The spectral energy distributions (SEDs) are fitted with the new version of the CIGALE code (Code Investigating GALaxy Emission, `http://cigale.lam.fr`) developed with PYTHON. CIGALE combines a UV-optical stellar SED with a dust component emitting in the IR and fully conserves the energy balance between the dust absorbed stellar emission and its re-emission in the IR. We refer to Burgarella et al. (in preparation) and Boquien et al. (in preparation) for a detailed description of the new version code. The earlier version of CIGALE is described in Noll et al. (2009). Here we only describe the assumptions and choices specific to the current study. The choice of the models and parameters is the result of a long process of optimization which will be fully discussed in Buat et al. (in preparation).

Table 2
Impact of the choice of the attenuation law and of considering IR data on the SFR and stellar masses ($M_{\rm star}$) determinations. The first part of the table summarises the comparison between the 3 different attenuation laws considered in this work, in the second part of the table the results of the fits with and without IR data are compared for each of the 3 attenuation laws

Models	log($M_{\rm star}$) dex	log(SFR) dex
with IR		
C00-B12	0.09±0.08	-0.03±0.14
SMC-B12	-0.02 ±0.05	-0.04 ±0.10
C00-SMC	0.11±0.10	0.01 ±0.19
without IR - with IR		
C00-C00	-0.03 ±0.11	0.14 ±0.30
B12-B12	-0.06 ±0.14	0.17 ±0.36
SMC-SMC	-0.06 ±0.14	0.11 ±0.38

For the star formation we adopt the fiducial model of Buat et al. (2014) which consists of two stellar populations: a recent stellar population with a constant SFR on top of an older stellar population created with an exponentially declining SFR (e-folding rate τ). Ages of the older stellar population and young component (t_f and $t_{\rm ySP}$ respectively) are free parameters. The two stellar components are linked by their stellar mass fraction $f_{\rm ySP}$.

We can run CIGALE with different scenarios for the dust attenuation. Our fiducial attenuation recipe is the one we obtained by studying high redshift galaxies (Buat et al. (2012), hereafter B12), it is close to the LMC2 extinction curve with a UV bump of moderate amplitude and a rather steep increase in the UV. We also consider the grayer attenuation law of Calzetti et al. (2000) (hereafter C00) and an SMC extinction curve (hereafter SMC). The amount of dust extinction is measured with $E(B-V)$. The main parameters and the range of the input values are reported in Table 1.

The templates used for the dust re-emission in the IR come from Dale et al. (2014) (used without any AGN contribution). With CIGALE, we can add the contribution of an AGN to the SED. The adopted templates are those of the Fritz et al. (2006) library. Our fiducial fits are performed with two models of type 2 AGN with a low or a high optical depth at 9.7 μm.

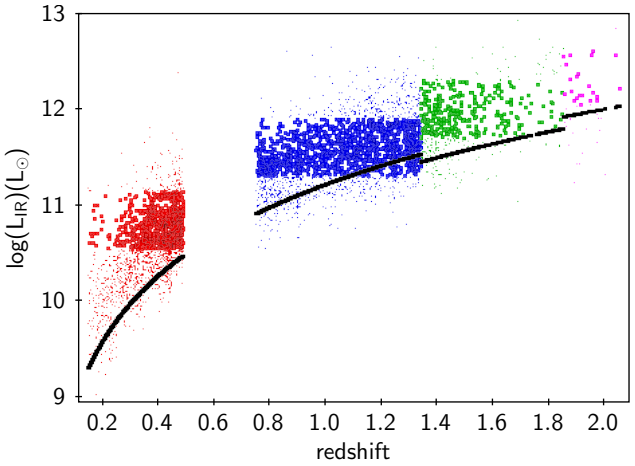

Figure 1. Redshift and luminosity distributions of the sources. The total IR luminosity $L_{\rm IR}$ is an output of the SED fitting. The small dots represent the whole sample and the filled circles the galaxies selected around $L^*_{\rm IR}$ within each redsfhift bin. The adopted values of $\log(L^*_{\rm IR})$ for the 4 redshift bins are 10.84, 11.6, 12 and 12.35 $L_\odot$, the bin size is 0.6 dex. Detection limits at 5σ are reported as a black line.

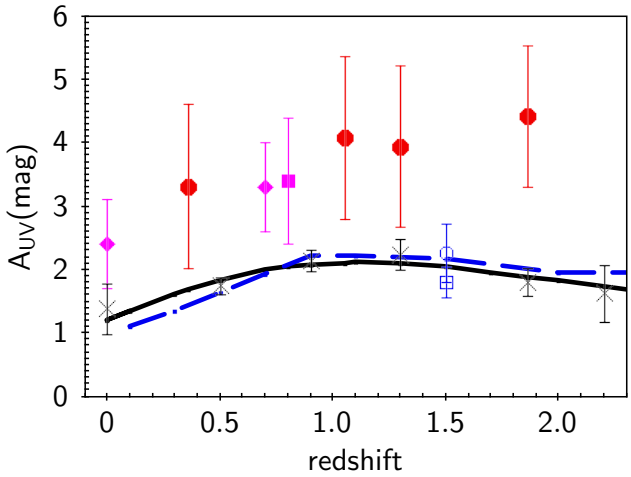

Figure 2. Dust attenuation in the UV ($A_{\rm UV}$) plotted against redshift . Red filled circles: present study with the selection around $L^*_{\rm IR}$ in each redshift bin. Magenta filled lozenges: Buat et al. (2007a,b); magenta filled square: Choi et al. (2006). The blue symbols refer to UV and H_α line selections. Blue dashed line: Cucciati et al. (2012); blue empty square: Heinis et al. (2013); blue empty circle: Ibar et al. (2013) . The global estimates of Burgarella et al. (2013) are plotted with black crosses and their average fit with a solid line The dispersion of each measurement is reported with a vertical bar.

The reduced χ^2_r distribution is found very good: for 93% of the sources the minimum value of χ^2_r is lower than 5, with a similar result for each redshift bin and for galaxies detected with PACS or not. The AGN fraction is of the order of 10% on average for the whole sample.

We explore the influence of the adopted attenuation curve and of the presence or not of IR ($\geq 8\mu$m) data on the determination of the SFR and stellar mass determination. The results are summarized in Table 2. In IR selected galaxies, the SFR is essentially constrained by the infrared emission from dust and does not depend much on the attenuation law. The stellar masses are found larger for the C00 attenuation law. The C00 curve exhibits the steepest increase in the UV and thus gives the lowest attenuation in the UV and the highest one in the V band since the total attenuation is constrained by $L_{\rm IR}$. Nevertheless the difference does not exceed ~ 0.1 dex.

Omitting or not IR data has large consequences on the measure of the SFRs whereas the stellar masses remain unaffected. This variation is due to the uncertainty on dust attenuation when IR data are missing. The average difference can reach 50% with a large dispersion (larger than a factor 2).

4. EVOLUTION OF DUST ATTENUATIOn

Our aim is to measure dust attenuation in galaxies selected in a similar way at different redshifts. The combination of the different IRC filters led us to perform a 8μm rest-frame selection. In Fig.1, $L_{\rm IR}$ (obtained with CIGALE) is reported against the photometric redshift of the sources. We have estimated the detection limit at 5σ using the flux limits of Murata et al. (2013) for each IRC filter used to define the sample and the average ratio between $L_{\rm IR}$ (found by SED fitting) and the monochromatic luminosity in the IRC filter corresponding to the redshift selection. It is clearly seen that we cannot follow galaxies with a similar $L_{\rm IR}$ over the full redshift range since the limit in luminosity increases sharply with z. We decide to study galaxies sampling the same domain of the luminosity function at the different redshifts. We select the galaxies dominating the luminosity function and therefore the luminosity density at a given redshift. At this aim, we take the total IR luminosity functions of Magnelli et al. (2013). In each redshift bin, we select galaxies with an IR luminosity inside a bin of 0.6 dex centered on the characteristic IR luminosity $L^*_{\rm IR}$ corresponding to the transition luminosity of the double power law function. The selection is also represented in Fig.1. It can be checked that the selected sources lie above the 5σ detection limit (except a small overlap at the end of the second redshift bin), the number of selected sources in each bin is 729, 1145, 284 and 24 from bin 1 to bin 4. The variation with redshift

of the attenuation is plotted in Fig.2.

We can first compare our measurements to other values already obtained for IR selected galaxies. At $z = 0$ Buat et al. (2007a) combined $GALEX$ and $IRAS$ data and derived volume averaged measures of the attenuation. For a luminosity $L^*_{\rm IR} \sim 10^{10.5} L_\odot$ (Sanders et al., 2003) the average UV attenuation $A_{\rm UV} = 2.4 \pm 0.7$ mag. Buat et al. (2007b) measured the attenuation of Luminous IR Galaxies ($L_{\rm IR} > 10^{11} {\rm L_{odot}}$) at $z = 0.7$ by combining *Spitzer* and $GALEX$ data and found a mean attenuation of 3.33 mag with a dispersion similar to that found at $z = 0$. Choi et al. (2006) also measured dust attenuation in galaxies of the *Spitzer* First Look Survey selected in mid-IR at $z = 0.8$ by comparing SFR measured with the strength of emission lines and $L_{\rm IR}$. We apply their relation between $A_{\rm V}$ and $L_{\rm IR}$ to the average value of $L_{\rm IR}$ of our sample at the same redshift and get $A_{\rm V} = 2.33$ mag. The visual extinction can then be translated to an attenuation in the UV continuum as explained in Buat et al. (2007b) giving $A_{\rm UV} = 3.4$ mag. The dispersion is directly measured on Fig.12 of Choi et al. (2006). All these previous measurements are overplotted on Fig.2 and are found consistent with the ones obtained in the present work which extents the analysis to higher redshift. The attenuation in the UV for $L^*_{\rm IR}$ galaxies is found to increase with redshift from 2.4 mag at $z = 0$ to 4.4 mag at $z \sim 2$.

We now compare the redshift evolution of the attenuation with measurements obtained in samples not selected in IR. Burgarella et al. (2013) measured the global attenuation in the universe by comparing the IR and UV luminosity densities. Their result is plotted in Fig.2. Measures of dust attenuation are also performed in UV selected samples. Cucciati et al. (2012) derived dust attenuation for each galaxy of their UV selection through SED fitting (without IR data), the variation they found is in close agreement with the results of Burgarella et al. (2013). Heinis et al. (2013) measured the average attenuation of a UV selection at $z \sim 1.5$ in the COSMOS field by stacking $Herschel$/SPIRE images. The average value found for their whole selection is consistent with the one derived by Cucciati et al. (2012) at the same redshift ($z = 1.5$). Ibar et al. (2013) analyzed the IR properties of galaxies detected in their Hα line (HIZELS project) at $z = 1.46$. From a stacking analysis of *Spitzer*, *Herschel* and AzTEC images they derived the average total IR luminosity of their sample and deduced a median attenuation of $A_{\rm H\alpha} = 1.2 \pm 0.2$ mag for their sample. This attenuation can be translated to the UV using the recipe of Calzetti (1997). The corresponding value (2.23±0.4 mag) is plotted in Fig.2 and is fully consistent with the other measures performed in a UV selection or globally with the luminosity functions.

The amount of attenuation found for our IR selection is much higher than the values found either in a UV selection or globally in the universe. When performing our IR selection we select galaxies dominating the star formation at the redshifts we consider. These galaxies are found to experience a dust attenuation much higher than the average one at work in the universe or found in UV selected samples: the galaxies dominating the star formation are not representative of the average attenuation and metal production in the universe.

Dust attenuation is found to depend on the stellar mass and the relation between these quantities is not found to significantly evolve with redshift (Ibar et al., 2013; Kashino et al., 2013; Heinis et al., 2014). We can use these relations to account for the stellar mass distributions when we compare dust attenuation from different selections. Let us consider the measure of Heinis et al. (2013) at $z \sim 1.5$: the average stellar mass for our IR selection in the redshift bin 3 is $10^{10.9} M_\odot$. Using the relation found by Heinis et al. (2014) between dust attenuation and M_{star}, we find that the average attenuation increases from 1.8 to 3.5 mag, leading to a value now consistent with the measures obtained in our IR samples.

The same exercise can be performed for the Hα selected sample. Using the relation of Kashino et al. (2013) between attenuation and stellar mass for Hα emitters we find $A_{\rm H\alpha} = 1.96$ mag which translates to 3.64 mag in the UV again consistent with what is found for our IR selected samples of similar mass.

Hence the stellar mass appears as the main driver to reconcile measures of dust attenuation in the different studies and explain the discrepancies between UV and IR selections as predicted by the empirical models of Heinis et al. (2014) and Bernhard et al. (2014).

ACKNOWLEDGMENTS

V. Buat and D. Burgarella acknowledge the support of offering visiting professor positions in 2013 from the Institute of Space and Astronautical Science. V. Buat is also supported by the grant of the Institut Universitaire de France.

REFERENCES

Bernhard, E., Béthermin, M., Sargent, M., et al., 2014, Modelling the connection between ultraviolet and infrared

galaxy populations across cosmic times, MNRAS, 442, 509

Buat, V., Takeuchi, T. T., Iglesias-Páramo, J., et al., 2007, The Local Universe as Seen in the Far-Infrared and Far-Ultraviolet: A Global Point of View of the Local Recent Star Formation, ApJS, 173, 404

Buat, V., Marcillac, D., Burgarella, D., et al., 2007, GOODS-Herschel: dust attenuation properties of UV selected high redshift galaxies, A& A, 469, 19 , A22

Buat, V., Noll, S., Heinis, S., et al., 2012, GOODS-Herschel: dust attenuation properties of UV selected high redshift galaxies, A&A, 545, 141

Buat, V., Heinis, S., Boquien, M., et al., 2014, Ultraviolet to infrared emission of z ¿ 1 galaxies: Can we derive reliable star formation rates and stellar masses?, A&A, 561, A39

Burgarella, D., Buat, V., Gruppioni, C., et al., 2013, The Local Universe as Seen in the Far-Infrared and Far-Ultraviolet: A Global Point of View of the Local Recent Star Formation, A&A, 554, A70

Calzetti, D., Armus, L., Bohlin, R. C., et al., 2000, The Local Universe as Seen in the Far-Infrared and Far-Ultraviolet: A Global Point of View of the Local Recent Star Formation, ApJ, 533, 682

Calzetti, D., 1997, Reddening and Star Formation in Starburst Galaxies, American Institute of Physics Conference Series, 408, 403

Choi, P. I., Yan, L., Im, M., et al., 2006, Star Formation Rates and Extinction Properties of IR-luminous Galaxies in the Spitzer First Look Survey, ApJ, 637, 227

Cucciati, O., Tresse, L., Ilbert, O., et al., 2012, A&A, The star formation rate density and dust attenuation evolution over 12 Gyr with the VVDS surveys, 539, A31

Dale, D. A., Helou, G., Magdis, G. E., et al., 2014, A Two-Parameter Model for the Infrared/Submillimeter/Radio Spectral Energy Distributions of Galaxies and AGN, ApJ, 784, 83

Fritz, J., Franceschini, A., & Hatziminaoglou, E., 2006, Revisiting the infrared spectra of active galactic nuclei with a new torus emission model, MNRAS, 366, 767

Goto, T., Takagi, T., Matsuhara, H., et al. 2010, Evolution of infrared luminosity functions of galaxies in the AKARI NEP-deep field. Revealing the cosmic star formation history hidden by dust, A&A, 514, A6

Heinis, S., Buat, V., Bethermin, M., et al., 2013, HERMES: unveiling obscured star formation - the far-infrared luminosity function of ultraviolet-selected galaxies at z 1.5, MNRAS, 429, 1113

Heinis, S., Buat, V., Bethermin, M., et al., 2014, HerMES: dust attenuation and star formation activity in ultraviolet-selected samples from z 4 to 1.5, MNRAS,

Ibar, E., Sobral, D., Best, P. N., et al., 2013, Herschel reveals the obscured star formation in HiZELS Halpha emitters at z = 1.47, MNRAS, 434, 3218

Kashino, D., Silverman, J. D., Rodighiero, G., et al., 2013, The FMOS-COSMOS Survey of Star-forming Galaxies at z 1.6. I. Halpha-based Star Formation Rates and Dust Extinction, ApjL, 777, L8

Magnelli, B., Popesso, P., Berta, S., et al., 2013, The deepest Herschel-PACS far-infrared survey: number counts and infrared luminosity functions from combined PEP/GOODS-H observations, A&A, 553, A132

Murata, K., Matsuhara, H., Wada, T., et al., 2013, AKARI North Ecliptic Pole Deep Survey. Revision of the catalogue via a new image analysis, A& A, 559, A132

Noll, S., Burgarella, D., Giovannoli, E., et al., 2009, Analysis of galaxy spectral energy distributions from far-UV to far-IR with CIGALE: studying a SINGS test sample, A&A, 507, 1793

Oi, N., Matsuhara, H., Murata, K., et al., 2014, Optical - near-infrared catalog for the AKARI north ecliptic pole Deep field, A&A, 566, A60

Sanders, D. B., Mazzarella, J. M., Kim, D.-C., Surace, J. A., & Soifer, B. T., 2003, The IRAS Revised Bright Galaxy Sample, AJ, 126, 1607